Stasiak et al., J Proteomics Bioinform 2017, 10:10
DOI: 10.4172/jpb.1000447

Journal of
Proteomics & Bioinformatics

Research Article OMICS International

Differential Quantitative Proteomics of Human Microvascular Endothelial Cells 1 by iTRAQ Reveals Palladin to be a New Biomarker During TGF- β 1 Induced Endothelial Mesenchymal Transition

Marta Stasiak[1*], Katarzyna Gawryś[1], Marcin Popielarski[1], Radosław Bednarek[1], Maciej Studzian[2], Ewa Sitkiewicz[3], Janusz Szemraj[4] and Maria Swiatkowska[1]

[1]*Department of Cytobiology and Proteomics, Medical University of Lodz, Poland*
[2]*Department of Molecular Biophysics, Faculty of Biology and Environmental Protection, University of Lodz, Poland*
[3]*Mass Spectrometry Laboratory, Institute of Biochemistry and Biophysics, Polish Academy of Sciences, Warsaw, Poland*
[4]*Department of Medical Biochemistry, Medical University of Lodz, Poland*

Abstract

The study uses global quantitative proteomics to investigate the molecular mechanisms behind the induction of endothelial-mesenchymal transition (EndMT) by transforming growth factor–β (TGF-β). Orbitrap Velos mass spectrometers and iTRAQ – a labeling-based analysis were used to perform a global and quantitative comparison of two proteomes of Human Microvascular Endothelial Cells-1 (HMEC-1) treated or not treated by TGF-β1. iTRAQ analysis identified 43 differentially-expressed proteins in the early stages of EndMT induced by TGF-β1. From 5522 identified proteins, 26 were downregulated and 17 were upregulated, including proteins such as palladin, POTE I, torsin A and nucleoporin (NDC1). Further analysis of palladin revealed its increased mRNA and protein expression in response to TGF-β and Snail transcription factor. Our findings demonstrate that the newly- identified proteins may be involved in early stages of biological processes leading to EndMT.

Biological Significance: Endothelial to mesenchymal transition is a possible source of myofibroblasts, which play a crucial role in the pathogenesis of fibrosis. EndMT participate in tissue fibrotic processes in various organs. TGF-β family growth factors are involved in the initiation of EndMT. The intracellular cascades activated by TGF-β that result in the remarkable phenotypic change of endothelial cells to mesenchymal cells have not been entirely elucidated. The downstream signaling pathway initiated by TGF-β resulted in a strong upregulation of the Snail1 transcriptional repressor. Our proteomics data demonstrated that TGF-β -induced EndMT leads to alterations in protein profiles, more specifically, the upregulation of palladin. This upregulation is mediated by Snail transcription factor and GSK-3 β signaling kinase. Our results also suggest that palladin could be considered a new biomarker in the early stages of cellular transdifferentiation, eventually leading to endothelial-mesenchymal transition.

Keywords: EndMT; Fibrosis; Palladin; Snail

Abbreviations: EndMT: Endothelial-Mesenchymal Transition; TGF-β: Transforming Growth Factor-β; iTRAQ: Isobaric Tags for Relative and Absolute Quantitation.

Introduction

Endothelial to mesenchymal transition (EndMT) is the process by which endothelial cells lose their cell-specific markers and morphology and acquire a mesenchymal cell-like phenotype. This process is regulated by a complex of several signaling pathways. EndMT plays a crucial role in the pathogenesis of various fibrotic diseases including interstitial pulmonary fibrosis, systemic sclerosis, as well as liver, heart and kidney fibrosis [1-4]. Elevated production and accumulation of collagen-rich extracellular matrix proteins occurs in various organs during the development and progression of pathological fibrosis, as well as in the stroma of many solid tumors [5-7]. Recent studies have shown that EndMT in the tumor microenvironment generates carcinoma-associated fibroblasts [8] and may be essential for cancer progression. Activated fibroblasts formed during cardiac, renal, and lung fibrosis are of endothelial origin [9-11]. EndMT has also been implicated in pulmonary hypertension, wound healing and tumor fibrosis. Recent findings have suggested that Snail1 mediates the actions of endogenous TGF-β 1 signalssignaling that induces EndMT [12]. Pathological expression of Snail genes can be observed in fibrotic areas, for example, in the human kidneys.

During EndMT, the endothelial cells lose markers, such as vascular-endothelial cadherin (VE-cadherin) and platelet endothelial cell adhesion molecule-1 (PECAM-1), and gain mesenchymal markers, such as α-smooth muscle actin (α-SMA), fibroblast specific protein-1 (FSP-1), neural-cadherin (N-cadherin) and vimentin. Resident endothelial cells leave the organized cell layer, lose cell–cell junctions, and acquire invasive and migratory properties. The TGF-β is a potent inducer of EndMT in several biological systems. In addition, it plays a crucial role in tissue fibrosis and is implicated in the pathogenesis of numerous fibrotic disorders [13].

Although several signaling pathways involved in TGF-β -induced EndMT have been identified to date, the precise mechanisms by which TGF-β converts an endothelial cell into a mesenchymal-like cell remain unclear. The aim of the present study is was to characterize the molecular mechanisms behind the early stages of EndMT by the quantitative proteomic analysis of cells EndMT.

***Corresponding author:** Marta Stasiak, Department of Cytobiology and Proteomics, Medical University of Lodz, Mazowiecka 6/8, Lodz, Poland, Tel: +48-422725724; E-mail: marta.stasiak@umed.lodz.pl

Received June 23, 2017; **Accepted** October 04, 2017; **Published** October 11, 2017

Citation: Stasiak M, Gawryś K, Popielarski M, Bednarek R, Studzian M, et al. (2017) Differential Quantitative Proteomics of Human Microvascular Endothelial Cells 1 by iTRAQ Reveals Palladin to be a New Biomarker During TGF-β1 Induced Endothelial Mesenchymal Transition. J Proteomics Bioinform 10: 236-245. doi: 10.4172/jpb.1000447

Materials and Methods

Cell culture

Human Microvascular Endothelial Cells (HMEC-1) initially obtained from human foreskins were transfected with a PBR 322-based plasmid containing the coding region for the simian virus 40 large T antigen. The cell line was immortalized by Dr. Edwin Ades and Mr. Francisco J. Candal, both of CDC, and Dr. Thomas Lawley, of Emory University. HMEC-1 cells were provided by Jason Goldstein, PhD from the Center for Disease Control and Prevention, Atlanta, GA, USA. The base medium for this cell line was MCDB131 (without L-Glutamine) supplemented with: 10 ng/mL Epidermal Growth Factor (EGF); 1 μg/mL Hydrocortisone; 2 mM L-glutamine; 10% Fetal Bovine Serum (FBS) and 100 units/ml Penicillin, 100 μg/ml Streptomycin. The cells reached 90% confluence in the culture flask, trypsin–EDTA was used to remove them, and the cells were used in experiments or reseeded in another flask. The cells were incubated at 37°C in a humidified atmosphere of 5% CO_2.

Protein extraction and quantification

Before the experiment, HMEC-1 cells were starved in OptiMEM® I for 24 hours. TGF-β1 was then added at a concentration of 5 ng/ml for 24 hours. The cells were next washed with Phosphate-buffered saline (PBS) and lysed with M-PER™ Mammalian Protein Extraction Reagent (Thermo Scientific™) on ice. After protein quantification using a BCA Protein Assay Kit (Pierce™), the proteins were precipitated, maintained in a with cold acetone for 24 hours at -20˚C, centrifuged and dried. Eight 100 μg samples (four controls and four samples after TGF-β1 treatment) were prepared for quantitative analysis.

Trypsin digestion of protein and iTRAQ labeling

The protein samples were reconstituted in 20 μl dissolution buffer with 0.1% sodium lauryl (dodecyl) sulfate (SDS) and sonicated. Next the disulfide bonds of the proteins were reduced with 50 mM tris-(2-carboxyethyl) phosphine (TCEP) for one hour at 60°C. The cysteine groups in the protein were then reversibly blocked by incubating with 200 mM methyl methanethiosulfonate (MMTS) in isopropanol for 10 minutes: these reagents were supplied as a part of the iTRAQ kit (Applied Biosystems).

The samples were digested overnight in trypsin (Promega) at 37°C on a rotary stirrer. After reconstitution, the digested peptides were labeled with another iTRAQ Reagent (113-121) for two hours at room temperature. Labeling was stopped by adding a sample buffer (8M urea, 0.002% bromophenol blue in 50 mM Tris-HCl, pH 8.0), according to the iTRAQ manufacturer's protocol. For LC-MS/MS experiment iTRAQ-labeled samples were combined and concentrated for the IPG strip (SpeedVac™ Concentrator).

The labeled peptides were separated according to the isoelectric point in Immobiline DryStrip gels (IPG strips). Each sample was applied to 18 cm IPG strip with 3–11 NL pH gradients (GE Healthcare) for isoelectrofocusing (IEF), using 340 μl of sample/strip, corresponding to 400 μg protein. The IPG strip was rehydrated overnight in an IPG box (GE Healthcare).

The next day, the strips were isoelectrofocused using an Ettan IPGphor 3 electrophoresis system (GE Healthcare) as follows. A five-hour pre-run was performed at 500V. Following this, a long gradient focusing program was used: one hour at 500 V, nine hours at 1000 V and 30 hours at 8000 V (the final current was 5 μA). After focusing, the strip was removed from the tray and the overlay oil was blotted with a paper tissue. Next, the strip was divided to 18 fractions and labeled peptides were eluted from the gel (2 x 60 μl of 0.1% TFA in 2% acetonitrile, one hour with stirring).

LC–MS/MS analysis using C18 reverse phase chromatography

The separated peptides were applied to a nanoACQUITY UPLC Trapping Column (Waters) and then transferred to a 75 μm inner diameter, 250 mm-long nanoACQUITY UPLC BEH C18 Column (Waters) with a flow rate of 250 nl/minute. Column outlet was directly coupled to the Electrospray ionization (ESI) ion source of the Orbitrap Velos type mass spectrometer (Thermo Scientific), working in the regime of data dependent MS to MS/MS switch with HCD type peptide fragmentation. Other Orbitrap parameters were as follows: one MS scan was followed by a maximum of five MS/MS scans. Capillary voltage was 1.5 kV, the results were acquired in a positive polarity mode. The MS/MS spectra of peptides of each fraction were measured over 18 runs of three hours each.

The acquired MS/MS data were pre-processed with Mascot Distiller software (v.2.3, MatrixScience) and a search was performed with the Mascot Search Engine MatrixScience, Mascot Server 2.4) against the set of Human protein sequences (20348 sequence) derived from Sprot database (541954 sequences; 192668437 residues). The search parameters were set as follows: enzyme, semitrypsin; fixed modification, cysteine modification by MMTS, as well as iTRAQ labeling of the N-terminus of peptides and of lysine side chains; variable modifications - oxidation (M); max missed cleavages – 1.

This procedure provided q-value estimates for each peptide spectrum match (PSM) in the dataset. All PSMs with q-values >0.01 were removed from further analysis. A protein was regarded as confidently identified if at least two of its peptides were found. Proteins identified by a subset of peptides from another protein were excluded from analysis. The proteins that exactly matched the same set of peptides were combined into a single cluster. The mass calibration and data filtering were carried out with the developed in-house MScan software (http://proteom.ibb.waw.pl/mscan/). The lists of peptides that matched the acceptance criteria from the LC-MS/MS runs were merged into one common list.

Statistical significance was assessed with the Diffprot in-house software package [14,15]. The software determines the statistical validity of the regulation/expression status of the protein represented by its calculated protein ratio, based solely on the statistical analysis of the datasets from a given experiment, without assumptions on the character of the distribution of peptide ratios in a dataset (e.g. its normality). The probability of obtaining a given protein ratio by random selection from the dataset was tested by calculating protein ratios for a large number of permuted decoy datasets in which the peptide-protein assignment was scrambled. Calculated p-values were adjusted for multiple testing using a procedure controlling for false discovery rate (FDR). Only proteins with a q-value below 0.05 or those present in only one of two compared analytical groups were taken into consideration during further analysis.

Immunoblotting

The protein content of lysates was determined by the BCA method. Cell lysate aliquots containing appropriate equal total protein were boiled with 5x concentrated sample buffer, separated by SDS PAGE then electrophoretically transferred to nitrocellulose membrane (BioRad). Proteins were detected with the anti - SM22 (Thermo) and anti- claudin 1 (Cell Signaling) polyclonal antibodies and the anti- Snail 1 (Cell Signaling), anti - palladin (Novus), anti- vimentin

(Sigma), anti - α-tubulin (Sigma) and HRP conjugate anti - GAPDH (Santa Cruz Biotechnology) monoclonal antibodies. Immunodetection was performed using an enhanced chemiluminescence kit (ECL Kit, PIERCE), with the resulting Kodak BioMax Light Films (Eastman Kodak, Rochester, NY, USA) scanned. The protein extracts and the control lysate from human Snail-transfected 293T cells (Santa Cruz Biotechnology) were used as controls.

Real-time PCR

Total RNA of HMEC-1 cells was isolated using Trizol® (Invitrogen) according to the manufacturer's instructions. Determination of RNA quality was performed on an Agilent 2100 Bioanalyzer (Agilent Technologies). Reverse transcription was performed at 50°C for 30 minutes with 1 μg of total RNA and the Maxima First Strand cDNA synthesis kit with double strand DNAse (Thermo Scientific). Real-time PCR experiments were performed on an Mx3005P thermocycler (Agilent Technologies) with Maxima SYBR Green/ROX qPCR Master Mix (Thermo Scientific) and specific primers for human Snail1, PECAM, VE-cadherin, FSP-1, integrin subunit α11 and SM22α (transgelin). Primer sequences and sizes of the PCR product for each targeted gene are described in Table 1. Each sample was normalized to the GAPDH housekeeping gene. The ΔΔCt method was used for the relative quantification. PCR assays were conducted in triplicate for each sample.

Confocal microscopy

HMEC-1 cells were seeded at a concentration of 1×10^4 cells per well on a 96-well SCREENSTAR microplate (Greiner Bio-One). After 24 hours, control and TGF-β1-stimulated cells were fixed using methanol-free 1% formaldehyde solution (Thermo Scientific Pierce) and blocked for one hour at room temperature using 3% BSA solution prepared in PHEM buffer (60 mM PIPES, pH 6.9, 25 mM HEPES, 10 mM EGTA, 4 mM $MgCl_2$). Subsequently, the cells were incubated overnight at 4°C with respective primary antibodies anti-PECAM conjugated with FITC (BD Pharmingen), anti-vimentin (Sigma), anti-Snail (Cell Signaling) diluted in 1% BSA/PHEM. Finally, cells were washed three times with PHEM buffer, stained for one hour at room temperature with respective secondary antibodies conjugated with Alexa Fluor 488 or Alexa Fluor 568 (Invitrogen) prepared in 1% BSA/PHEM and again washed three times with PHEM buffer. Cell nuclei were counterstained for 15 minutes with 5 μM Hoechst33342 dye, and the cells were stored refrigerated and protected from light in PHEM buffer until imaging.

Genes	Primer Sequences
α11	F: CACGACATCAGTGGCAATAAG
	R: GACCCTTCCCAGGTTGAGTT
Claudin-1	F: TTGACTCCTTGCTGAATCTGAG
	R: TTCTGCACCTCATCGTCTTC
GAPDH	F: CCATCACCATCTTCCAGGAGCG
	R: GAGAGATGATGACCCTTTTGGC
FSP-1	F: ACTTGGACAGCAACAGGGAC
	R: GCTGCTTATCTGGGAAGCCT
PECAM	F: GACGTGCAGTACACGGAAGT
	R: TCTGCTTTCCACGGCATCAG
Snail	F: GCT GCA GGA CTC TAA TCC AGA
	R: ATC TCC GGA GGT GGG ATG
SM22 α	F: TCAGATGGGCAGCAACAGAG
	R: GCCAAGGCAGTGATGCTTTC
VE-Cadherin	F: TGGTCACCCATGCATCTTCC
	R: CCATGACGAAGGGTGAGCTT

Table 1: PCR primer sequences.

All confocal microscopy images were obtained under 6300x magnification with an LSM780 microscope equipped with a Plan-Apochromat 63x/1,4 Oil DIC M27 objective, 405 nm laser diode and InTune™ tunable excitation laser system (Carl Zeiss; Oberkochen, Germany).

Statistical analysis

Data are presented as mean ± standard deviation. The results were repeated with at least three independent experiments. Statistical analyses were performed using unpaired *t*-test for two-group comparisons and the Tukey test following one-way ANOVA test for multiple groups.

Results

TGF-β regulates the expression of mesenchymal markers

To better understand the role of TGF-β signaling in initiating EndMT, TGF-β -induced proteomic changes were identified in a line of human dermal microvascular endothelial cells (HMEC-1) using global quantitative proteomics methods. HMEC-1 express various endothelial markers, including PECAM, and Claudin1, whereas mesenchymal cells express others: transgelin (SM22α), vimentin, fibronectin, collagens and smooth muscle cell actin (SMA). Several transcription factors are involved in EndMT transition, including the Snail repressor. HMEC-1 were treated for 48 hours with TGF-β1 at concentrations ranging from 1 to 50 ng/ml after 24 hours serum starvation (Figure 1A). Stimulation of HMEC-1 cells with TGF-β1 induced expression of Snail transcription factor, which was confirmed by immunoblotting (Figure 1A) and Real-time quantitative PCR (Figure 1B).

TGF-β1 was found to have a dose-dependent effect on the expression of Snail1. The highest level of Snail was reached in the presence of 10 ng/ml of TGF-β1. The initial changes in the Snail expression were observed at a TGF-β1 concentration of 5 ng/ml, which was then used in the following experiment. Real-time quantitative PCR examination found that HMEC-1 treated with 5 ng/ml TGF-β1 for 24 or 48 hours increased Snail mRNA levels (Figure 1C).

Light microscope morphological examination of HMEC-1 revealed a slight change from an endothelial morphology to fibroblast-like morphology following treatment with TGF-β1 for 48 hours (Figure 1D). No significant changes in cell morphology were observed in early stages of EndMT.

Immunoblotting was performed to assess the protein expression of the endothelial markers: VE cadherin, claudin1 and the mesenchymal markers: vimentin, SM22α and α11 integrin, as well as the control markers: tubulin and GAPDH. TGF-β1 treatment caused decreased protein expression of VE cadherin and claudin-1, greater expression of SM22α and vimentin, and slightly elevated expression of α11integrin (Figure 2A).

Real-time quantitative PCR was performed to assess gene expression of endothelial markers (claudin1, PECAM, VE-cadherin) and mesenchymal markers (FSP-1, α11, SM22α) in HMEC1 treated by TGF-β1 (Figure 2B). Treatment of HMEC-1 with TGF-β1 for 48 hours confirmed decreased levels of endothelial markers and increased expression of mesenchymal markers.

Finally confocal microscope examination found that TGF-β1 induced mesenchymal marker expression and decreased endothelial marker expression. To detect the endothelial marker (PECAM) and the mesenchymal marker (vimentin), the cells were stimulated with TGF-β1 for 24 hours and then treated with anti-PECAM antibody

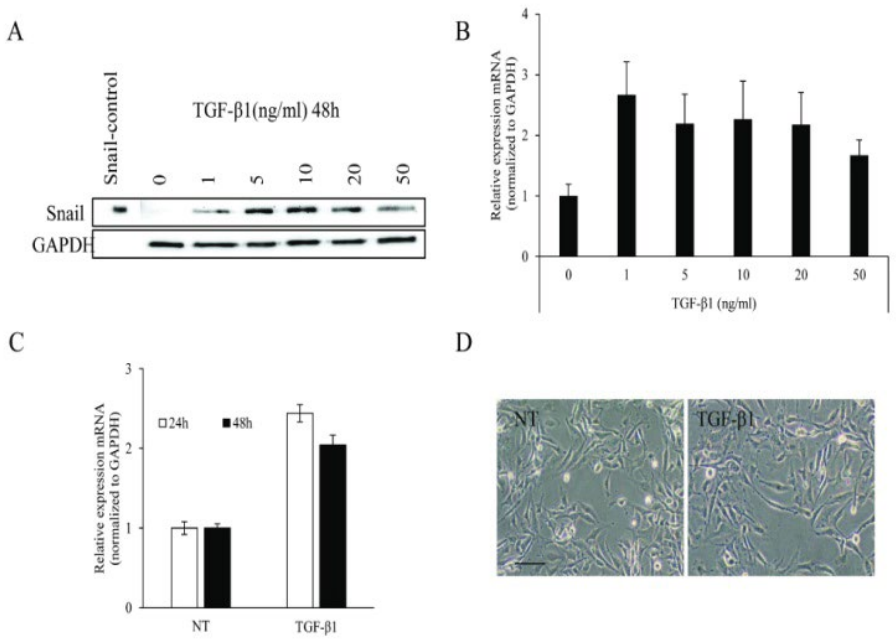

Figure 1: (A) Western blot analysis of Snail expression in TGF-β1 treated HMEC-1 cells. Upper numbers indicate the value by densitometry normalized to control. (B and C) Quantitative RT-PCR analysis of Snail mRNA levels normalized to GAPDH in HMEC-1 cells depending on the time of stimulation (C) and concentration (B) of TGF-β1. Data are presented as mean ± SD from three independent experiments. Significance of statistical differences between control and treated TGFβ1 is at P<0.05. (D) Morphology (representative pictures) of HMEC-1 cells treated and untreated with TGF-β1 as observed by phase contrast microscopy (scale bar, 10 μm).

conjugated with FITC or with anti-vimentin antibody, followed by a secondary antibody conjugated with Alexa Fluor (Figure 2C). This application of TGF-β1 was found to be sufficient to induce EndMT.

Analysis of differentially expressed proteins during TGF-β1 induced EndMT in HMEC-1

iTRAQ labeling followed by nL-LC-MS/MS analysis, with Orbitrap Velos mass spectrometers, was used to quantitatively profile global protein expression. The peptides were labeled with isobaric chemical tags and a global quantitative comparison of two proteomes was performed using a total number of 5522 proteins. A total of 43 proteins were observed to be significantly differentially expressed between the treated and untreated samples (P<0.05). Of these, 17 were overexpressed and 26 were down-regulated after TGF-β1 stimulation (Table 2).

Of the 17 up-regulated proteins (Table 2A), nucleoporin NDC1, POTE I, torsin A and palladin are of special interest for the biology of EndMT. Of the 26 down-regulated proteins (Table 2B) debrin-like protein (DBNL) and alpha crystallin B (αB crystallin) were of interest. Some of the down-regulated proteins, such as STAT1, IFIT3, IFIT1, GBP1, OAS2, OAS3, ISG15, UBE2L6, MX1 and DDX58, can be involved in negative regulation of EndMT.

Biological function

Proteomic analysis was used to determine the distribution of overexpressed proteins according to biological processes. Of the 5522 identified proteins, only 43 were significantly modulated by TGF-β 1 treatment (P<0.05). The functional significance of the proteins, their localization in cellular components (Figure 3) and their possible role in biological processes (Figure 4) were examined during 24-hour TGF-β1 treatment.

A search of the String 10.0 database (Search Tool for Analysis of Interacting Gens/Proteins) found the identified proteins to be involved in a number of biological processes, including response to stimulus (POTEI, AKAP12, DAB2, DBNL, DDX58, OAS2, OAS3), response to stress (DBNL, DDX58, OAS2, OAS3, MX1, POTE I, STAT1, STIP1), cellular response to cytokine stimulus (GBA, GPBP1, IFTI1, ISG1, MX1, STAT1), the cytokine-mediated signaling pathway (IFTI1, IFTI3, ISG15, MX1, STAT1). TGF-β1 mediates reorganization in cytoskeleton during EndMT, which is expressed as dynamic changes in cell morphology. The identified upregulated proteins are components of cell junctions (PALLD, AKAP12, DAB2, DBNL, DDX58, TOR1A, LAP3, LASP1, LIMA1), cytoskeleton (DBNL, DDX58, POTEI, PALLD, MYO1D, SLC2A1) and play a role in focal adhesion (AKAP12, DAB2, PALLD, LAP3, LASP1) (Figure 4). The upregulated proteins: palladin, POTEI and torsin A participate in the regulation of cytoskeleton reorganization.

Protein-protein interaction proteomic network analysis

String10.0 was also used for functional interpretation of the differentially expressed proteins for cellular processes. Direct interaction network analysis revealed interactions between. PALLD, POTEI, DBNL and MYO1D, which are involved in initiation of fibrosis, cancerogenesis, cell migration and cytoskeleton reorganization (Figure 5). Moreover, direct interactions were also identified between several proteins which were found to be downregulated, including STAT1, IFIT3, IFIT1, GBP1, OAS2, OAS3, ISG15, UBE2L6, MX1 and DDX58. These results suggest that these proteins may be involved in the negative regulation of early stages of EndMT initiated by TGF-β 1. Interestingly, although POTEI was upregulated, it was found to interact with some downregulated proteins (OAS2, OAS1, MX1, ISG15) following TGF-β 1 stimulation.

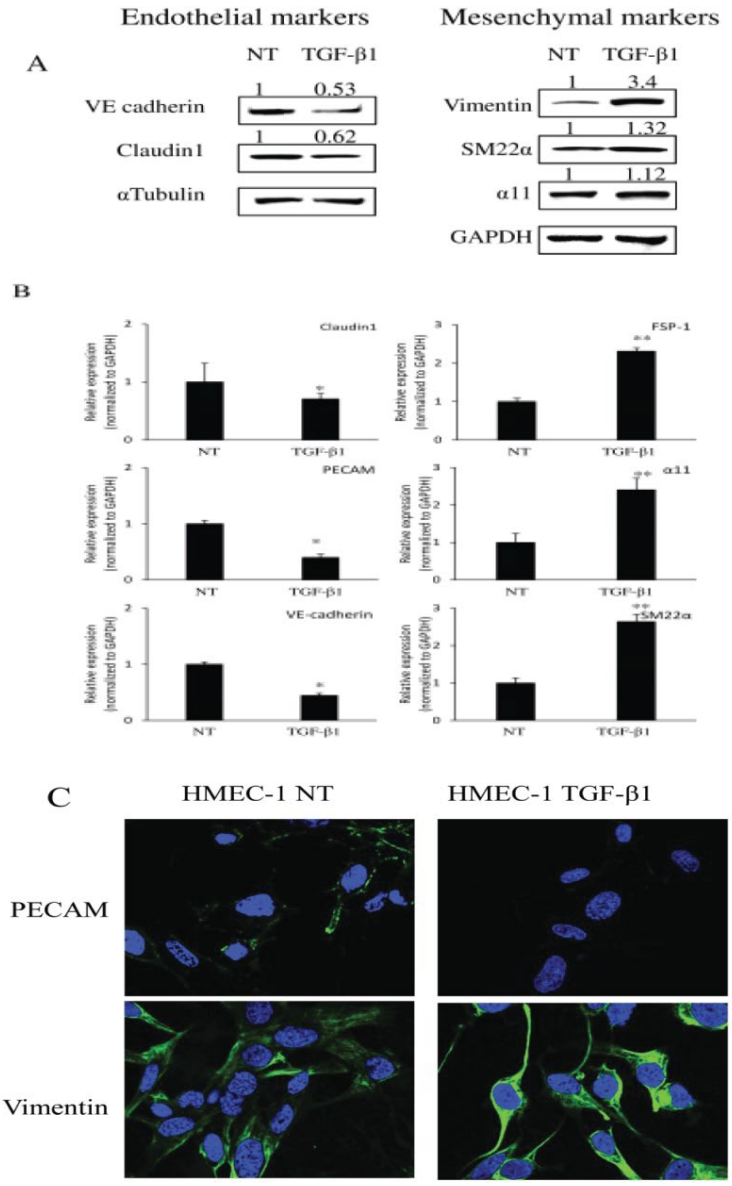

Figure 2: (A) Western blot analysis of VE-cadherin, claudin1, vimentin, SM22α and α11 expression in control and TGF-β1 treated for 48 hours HMEC-1 cells. Upper numbers indicate the value by densitometry normalized to control. The blots are representative of three independent experiments. (B) Relative claudin1, PECAM, VE-cadherin, FSP-1, α11, and SM22α mRNA expression in control (NT) and TGF-β1 treated HMEC-1 cells. Results shown as mean with SD. Asterisk (*) indicates statistically significant differences between control and treated TGFβ1 cells) (* P<0.05; ** P<0.01). (C) Subcellular location and expression level of vimentin and PECAM in TGF-β1 treated and untreated (NT) HMEC-1 cells examined by immunofluorescence and shown as representative confocal microscopy images (green pseudocolor). Cell nuclei (blue pseudocolor) were counterstained with Hoechst33342 dye.

A								
No	**Protein**	**Protein score**	**Coverage**	**Qvalue**	**Ratio**	**Fold change**	**Peptides**	**Description**
1	P50443	292	9.34	0.00053	1.57	1.57	6	Sulfate transporter OS=Homo sapiens GN=SLC26A2
2	Q9Y241	186	25.81	0.0072	1.5	1.5	3	HIG1 domain family member 1A, mitochondrial OS=Homo sapiens GN=HIGD1A
3	Q9HCJ1	130	9.15	0.02238	1.47	1.47	3	Progressive ankylosis protein homolog OS=Homo sapiens GN=ANKH
4	P11166	361	12.4	0.00391	1.45	1.45	6	Solute carrier family 2, facilitated glucose transporter member 1 OS=Homo sapiens GN=SLC2A1
5	Q9BTX1	229	7.86	0.00873	1.39	1.39	4	Nucleoporin NDC1 OS=Homo sapiens GN=NDC1
6	Q9NUN7	203	6.74	0.04612	1.39	1.39	3	Alkaline ceramidase 3 OS=Homo sapiens GN=ACER3

7	Q9NR50	101	9.51	0.01994	1.29	1.29	4	Translation initiation factor eIF-2B subunit gamma OS=Homo sapiens GN=EIF2B3
8	O14656	748	24.1	0.01899	1.27	1.27	8	Torsin-1A OS=Homo sapiens GN=TOR1A
9	P0CG38	13567	14.14	0.04126	1.24	1.24	5	POTE ankyrin domain family member I OS=Homo sapiens GN=POTEI
10	Q8WX93	306	7.45	0.00168	1.23	1.23	9	Palladin OS=Homo sapiens GN=PALLD
11	O94832	289	8.55	0.04409	1.19	1.19	6	Unconventional myosin-Id OS=Homo sapiens GN=MYO1D
12	O75531	1600	46.07	0.04191	1.18	1.18	8	Barrier-to-autointegration factor OS=Homo sapiens GN=BANF1
13	P05141	5270	44.63	0.04894	1.17	1.17	7	ADP/ATP translocase 2 OS=Homo sapiens GN=SLC25A5
14	Q70CQ2	859	4.31	0.01846	1.15	1.15	11	Ubiquitin carboxyl-terminal hydrolase 34 OS=Homo sapiens GN=USP34
15	P04062	856	23.32	0.02935	1.15	1.15	10	Glucosylceramidase OS=Homo sapiens GN=GBA
16	O60701	1439	40.49	0.04184	1.13	1.13	17	UDP-glucose 6-dehydrogenase OS=Homo sapiens GN=UGDH
17	Q9Y617	754	31.08	0.03203	1.1	1.1	14	Phosphoserine aminotransferase OS=Homo sapiens GN=PSAT1

B

No	Protein	Protein score	Coverage	Qvalue	Ratio	Fold change	Peptides	Description
1	P20591	6096	54.98	0.00053	0.66	1.52	31	Interferon-induced GTP-binding protein Mx1 OS=Homo sapiens GN=MX1
2	P05161	1103	67.27	0.00053	0.68	1.47	7	Ubiquitin-like protein ISG15 OS=Homo sapiens GN=ISG15
3	P02511	205	17.71	0.00222	0.7	1.44	4	Alpha-crystallin B chain OS=Homo sapiens GN=CRYAB
4	P29728	246	8.48	0.00148	0.71	1.4	5	2'-5'-oligoadenylate synthase 2 OS=Homo sapiens GN=OAS2
5	P09914	608	21.76	0.00053	0.74	1.35	9	Interferon-induced protein with tetratricopeptide repeats 1 OS=Homo sapiens GN=IFIT1
6	P32455	726	17.74	0.00082	0.75	1.33	6	Interferon-induced guanylate-binding protein 1 OS=Homo sapiens GN=GBP1
7	O14933	589	26.8	0.04171	0.77	1.3	4	Ubiquitin/ISG15-conjugating enzyme E2 L6 OS=Homo sapiens GN=UBE2L6
8	P30685	1230	32.6	0.00222	0.78	1.29	5	HLA class I histocompatibility antigen, B-35 alpha chain OS=Homo sapiens GN=HLA-B
	P30491	1230	32.6					HLA class I histocompatibility antigen, B-53 alpha chain OS=Homo sapiens GN=HLA-B
	P10319	1250	33.43					HLA class I histocompatibility antigen, B-58 alpha chain OS=Homo sapiens GN=HLA-B
9	Q15847	697	69.74	0.03273	0.79	1.26	4	Adipogenesis regulatory factor OS=Homo sapiens GN=ADIRF
10	Q9Y3Z3	1603	35.14	0.00053	0.8	1.25	19	Deoxynucleoside triphosphate triphosphohydrolase SAMHD1 OS=Homo sapiens GN=SAMHD1
11	O14879	452	27.35	0.01977	0.8	1.26	5	Interferon-induced protein with tetratricopeptide repeats 3 OS=Homo sapiens GN=IFIT3
12	P42224	4026	45.47	0.00053	0.81	1.23	28	Signal transducer and activator of transcription 1-alpha/beta OS=Homo sapiens GN=STAT1
13	P67809	2499	47.22	0.00185	0.81	1.23	10	Nuclease-sensitive element-binding protein 1 OS=Homo sapiens GN=YBX1
14	O95786	364	10.92	0.00082	0.83	1.2	8	Probable ATP-dependent RNA helicase DDX58 OS=Homo sapiens GN=DDX58
15	Q9UHB6	473	16.34	0.04216	0.84	1.19	8	LIM domain and actin-binding protein 1 OS=Homo sapiens GN=LIMA1
16	Q08380	72	6.15	0.03776	0.85	1.17	5	Galectin-3-binding protein OS=Homo sapiens GN=LGALS3BP
17	Q9Y6K5	439	12.33	0.01797	0.86	1.16	8	2'-5'-oligoadenylate synthase 3 OS=Homo sapiens GN=OAS3
18	P98082	655	12.73	0.04608	0.87	1.15	8	Disabled homolog 2 OS=Homo sapiens GN=DAB2
19	Q63HN8	3192	11.22	0.00053	0.88	1.14	51	E3 ubiquitin-protein ligase RNF213 OS=Homo sapiens GN=RNF213
20	Q14847	1989	51.72	0.01873	0.88	1.13	23	LIM and SH3 domain protein 1 OS=Homo sapiens GN=LASP1
21	Q06323	3855	64.26	0.028	0.88	1.13	20	Proteasome activator complex subunit 1 OS=Homo sapiens GN=PSME1
22	P28838	2894	47.01	0.00873	0.89	1.12	22	Cytosol aminopeptidase OS=Homo sapiens GN=LAP3
23	Q9UJU6	818	21.86	0.00851	0.9	1.12	12	Drebrin-like protein OS=Homo sapiens GN=DBNL
24	O00151	1528	48.63	0.01873	0.9	1.11	16	PDZ and LIM domain protein 1 OS=Homo sapiens GN=PDLIM1
25	Q02952	6553	34.79	0.00466	0.91	1.1	35	A-kinase anchor protein 12 OS=Homo sapiens GN=AKAP12
26	P31948	1783	39.41	0.02046	0.93	1.07	30	Stress-induced-phosphoprotein 1 OS=Homo sapiens GN=STIP1

Table 2: List of proteins in HMEC-1 found to be significantly differentially expressed in response to TGF-β1 by iTRAQ analysis. (A) up-regulated (B) down-regulated.

Enhanced expression of Palladin potentially contributes to TGF-β induced EndMT

Among the 17 proteins found to be upregulated following TGF-β 1 treatment, palladin is of particular interest (Figure 6). Differential expression was confirmed using Western blotting. The HMEC-1 cells were cultured in absence or presence of 5 ng/mL of TGF-β1 for 48 hours. Cells were starved of serum for 24 hours prior to TGF-β1 treatment. The cell lysates were prepared and analyzed for palladin. GAPDH expression was used to allow equal loading of all proteins. The expression of palladin at the protein (Figure 6D) and mRNA (Figure 6A) levels was found to be significantly increased following TGF-β1 treatment.

Snail regulates Palladin expression

Recent studies have revealed that Snail transcription factors are involved in EndMT. The downstream signaling pathway initiated by TGF-β resulted in strong upregulation of the transcriptional repressor

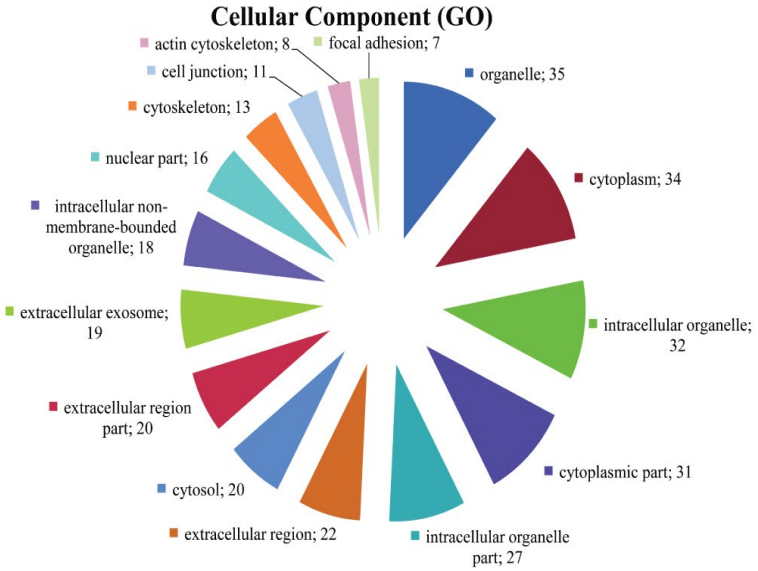

Figure 3: Classification of differently expressed proteins with numbers of respective proteins according to the cellular localizations Gene Ontology (GO). The analysis was performed using the String 10.0 database with a minimum false discovery rate P_{FDR}<0.05. The numbers refer to the number of proteins corresponding to the respective GO terminology.

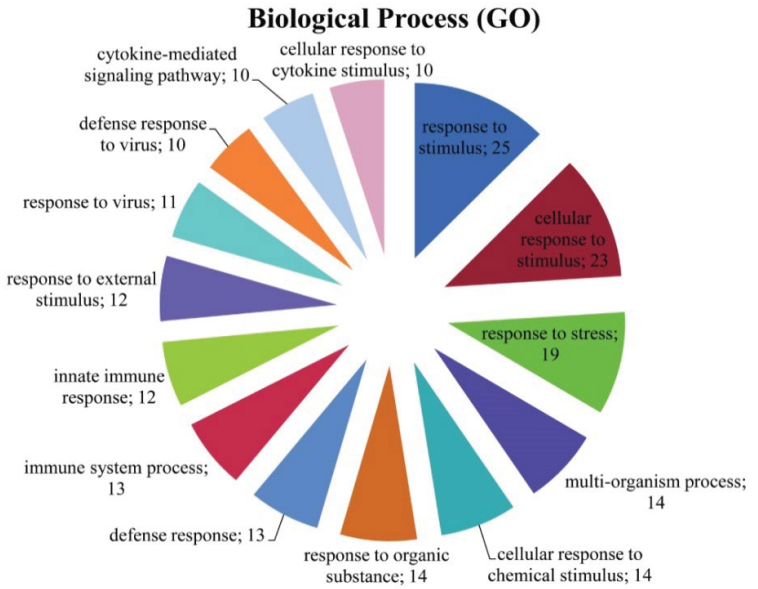

Figure 4: Occurrence of biological processes assigned to our EndMT model. The analysis was performed using the Siring 10.0 database. The numbers refer to the number of proteins corresponding to the respective GO term.

Snail. To determine whether Snail expression has an effect on palladin induction, HMEC-1 were transfected with a pcDNA-Snail expression plasmid for 48 hours. Snail expression was found to increase in cells transfected with the Snail expression vector (Figure 6G). No significant changes in palladin expression were observed at the protein level (Figure 6E); however, increased mRNA levels were found in cells transfected with the Snail expression plasmid (Figure 6B).

Overexpression of Snail was sufficient to induce EMT (epithelial to mesenchymal transition), but Snail expression alone was insufficient for EndMT. The Snail inhibitor GSK-3β needs to be inhibited by phosphorylation with a kinase such as AKT to induce EndMT. To determine whether inhibition of GSK-3β leads to increased expression of palladin, a chemical inhibitor of GSK-3β, lithium chloride (LiCl), was used. Cells transfected with Snail expression plasmid and then treated with LiCl show increased palladin expression at both the protein (Figure 6C) and mRNA levels (Figure 6F). These results suggest that the GSK-3β inhibition was involved in the up regulation of palladin expression by the Snail transcription factor and by the EndMT process.

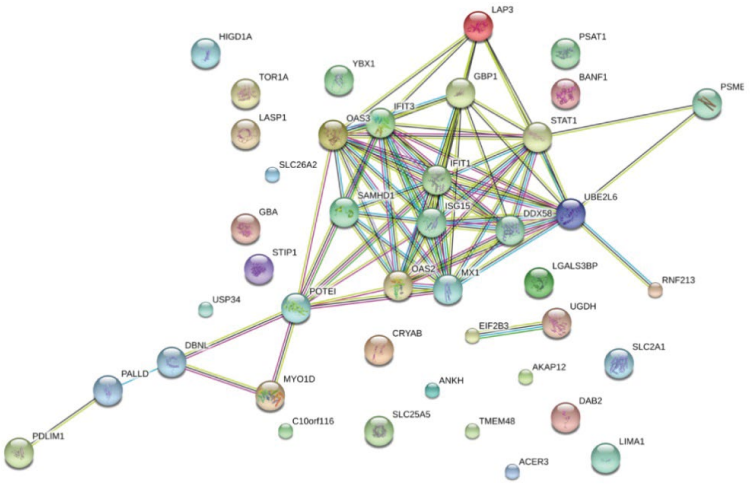

Figure 5: Biological network analysis of differentially expressed proteins in response to TGF-β1 by String pathway mapping tool. Direct interaction network of differentially expressed proteins identified by iTRAQ analysis in response to TGF-β1 treatment. The lines connecting the nodes indicate only direct binding protein-protein interactions. Protein names for nonobvious symbols are as follows: STAT1 (signal transducer and activator of transcription 1), IFIT3 (interferon-induced protein with tetratricopeptide repeats 3), GBP1 (interferon-induced guanylate-binding protein 1), DDX58 (probable ATP-dependent RNA helicase), IFIT1 (interferon-induced protein with tetratricopeptide repeats 1), UBE2L6 (ubiquitin/ISG15-conjugating enzyme E2 L6), ISG15 (ubiquitin-like protein ISG15), MX1 (interferon-induced GTP-binding protein Mx1), OAS3 (2'-5'-oligoadenylate synthetase 3), OAS2 (2'-5'-oligoadenylate synthetase 2), POTEI (POTE ankyrin domain family member I), MYO1D (unconventional myosin-Id), DBNL (drebrin-like protein), SLC2A1 (solute carrier family 2, facilitated glucose transporter member 1).

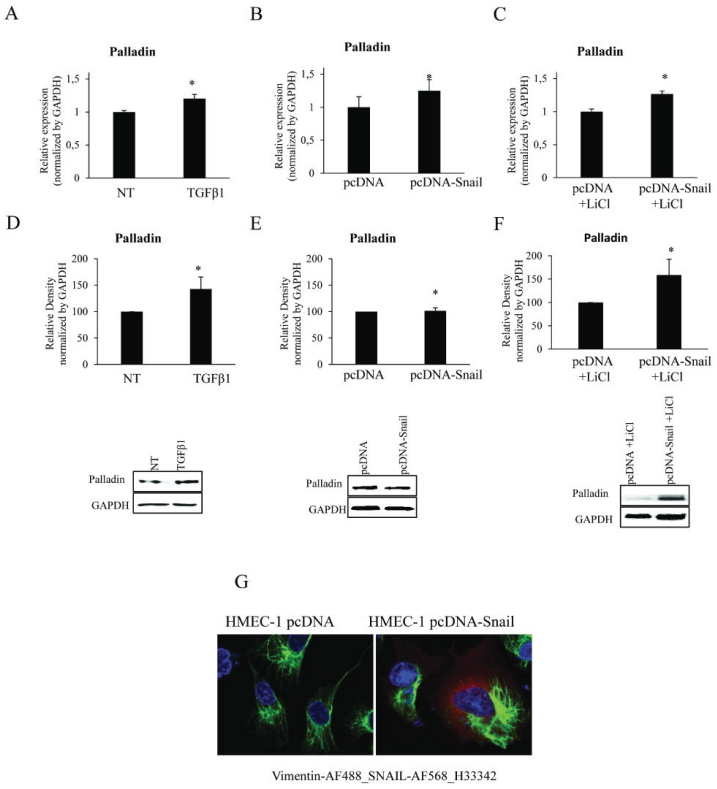

Figure 6: Quantitative RT-PCR analysis of palladin mRNA levels normalized to GAPDH in HMEC-1 cells: not treated and treated with TGFβ1 (A), transiently transfected with pcDNA or pcDNA-Snail (B), transiently transfected with pcDNA or pcDNA-Snail and next treated with LiCl (C). Western blot analysis of palladin expression in HMEC-1 cells: TGFβ1 treated (D) and transiently transfected with Snail (E), transiently transfected with Snail and treated with LiCl (F) (Data are presented as mean ± SD from three independent experiments. Asterisk (*) indicates statistically significant differences between control and treated TGFβ1 cells) (* $P<0.05$). (G) Subcellular location of vimentin (green pseudocolor) and Snail (red pseudocolor) in HMEC-1 cells transfected with pcDNA and pcDNA-Snail examined by immunofluorescence and shown as representative confocal microscopy images. Cell nuclei (blue pseudocolor) were counterstained with Hoechst33342 dye.

Discussion

Our data provides a novel insight into the molecular mechanisms that mediate early stages of EndMT. The results of the iTRAQ method highlight differences in protein profile between HMEC-1 cells treated with TGF-β1 and those untreated control cells. TGF-β1 treatment was found to promote the expression of 17 proteins, four of which are essential for inducing EndMT: palladin, torsin A, nucleoporin –NDC1 and POTE I. Furthermore, TGF-β1 increases the expression of the Snail transcription factor, which then activates the pathway leading to palladin expression.

Recent studies have highlighted the involvement of the TGF-β family of growth factors in the initiation of EndMT, but the molecular and the intracellular pathways activated by TGF-β that result in EndMT still remain unclear. Studies on primary murine pulmonary endothelial cells [16] and cultured human dermal microvascular cells [17] have demonstrated that EndMT involves both Smad-dependent and Smad-independent pathways. The molecular mechanism inducing EndMT by TGF-β has been found to involve the Snail family of transcription repressors. In mouse embryonic stem cell-derived endothelial cells, TGF-β induced EndMT and Snail expression [11].

Four proteins, which may be important in the biology of End MT, were chosen: NDC1, POTE I, torsin A and palladin. Nucleoporin 1 (NDC1) level was found to be up-regulated following 48-hour TGF-β 1 treatment. The proteomic analysis indicated significant, 1.39-fold upregulation of nucleoporin NDC1. Upregulation of nucleoporin NDC1 in the early stages of EndMT may suggest that it plays a role in progression. The nuclear envelope contains thousands of pores, these being sites for the movement of molecules between nucleus and cytoplasm determined by large macromolecular assemblies known as nucleopore complexes (NPC) [18]. The NPC consists of more than 30 evolutionarily conserved nucleoporins, each with a particular localization within nuclear envelope [19-21]. TGF-β induces the phosphorylation of the Smad proteins and drives Smads into the nucleus via the nuclear pore complex (NPC) [22,23]. The proteomic profile data revealed increased expression of one nucleoporin isoform, nucleoporin1 (NDC1), which confirms that Smad-dependent pathways are induced by TGF-β1 in the early stages of EndMT.

POTE I (POTE ankyrin domain family, member I) is another newly identified antigen overexpressed in EndMT transition. In humans the POTE gene family consists of 13 highly homologous members located on eight different chromosomes [24]. Previous studies have shown that POTE molecules are localized in the cytoplasm towards the inner part of the cellular membrane. POTE E is a dominant subtype expressed in many cancers including those of the prostate, colon, lung, breast, ovary, and pancreas and many as well as in numerous cancer cell lines [25,26]. POTE proteins expressed in cancer may have roles in cytoskeletal structure [27] but their exact function is unknown.

The next newly-identified protein upregulated by TGF-β1 in HMEC-1 is torsin A: a member of the AAA+ ATPase superfamily located within the lumen of the nuclear envelope and endoplasmic reticulum, which interacts with transmembrane proteins [28]. Torsin A is associated with laminin-associated polypeptide 1 (LAP1), conventional kinesin light chain 1 (KLC1), vimentin and actin. Torsin A occurs in complex with nesprin-plectin-vimentin in fibroblast and also has a role in nuclear dynamics *via* its association with nesprins and cytoskeleton. Torsin A was found to be associated with the cytoskeleton in fibroblasts by interaction with vimentin [29].

Significant overexpression of palladin was observed in the HMEC-1 cells transfected with Snail expression vector or treated by TGF-β1. The important changes in palladin expression during stimulation by TGF-β1 may represent an essential step in determining the morphology and actin organization of endothelial cells in EndMT transition.

Palladin is a multi-domain, actin-binding protein which binds directly to F-actin and many other actin-binding proteins, including profilin, VASP, ezrin, Lasp-1, EPS8, CLP-36, α-actinin and ArgBP2 [30-37]. Palladin is a cytoskeletal protein that controls stress fiber integrity, and is expressed in epithelial and mesenchymal cells [38,39].

TGF-β induced upregulation of palladin is mediated by Smad and mitogen-activated protein kinase pathways [38]. The downregulation of palladin leads to the disruption of actin-containing stress fibers, whereas upregulation leads to re-organization of the actin cytoskeleton and induction of thick actin bundles [38]. Palladin levels are up-regulated in metastatic cancer cells and play an important role in organizing actin arrays within migrating cells and in invasive motility [32]. The palladin gene was found within a cluster of invasion-specific genes in pancreatic and colorectal cancers [40-42]. The palladin protein levels increase significantly in human dermal fibroblasts in response to TGF-β 1 treatment, and during myofibroblast differentiation in the presence of TGF-β1 [39]. TGF-β increased palladin expression in human corneal fibroblasts in a manner dependent on Smad and MAPK signaling. Moreover, palladin was required for the TGF-β–induced upregulation of α-SMA [43]. Palladin activates fibroblasts inducing them to become myofibroblasts. The tumor-associated fibroblasts express palladin very early in tumorigenesis. In the early stages of neoplastic progression in pancreatic tumorigenesis, palladin expression levels in stromal fibroblasts increased and co-localized with α-SMA [44]. Palladin was found to be overexpressed in cancer-associated fibroblasts of different types of tumors such as pancreas, breast, lung, kidney, and ovary, promoting their invasion and metastasis [39].

Our findings very are the first to indicate that palladin is involved in the early stages of EndMT in HMEC-1 treated by TGF-β1. The upregulation of palladin is mediated by the Snail and GSK- β signaling pathways. Therefore, palladin may act as a potential biomarker in the early stages of EndMT.

Conclusion

Our study demonstrated that exposure of HMEC-1 to TGF-β 1 induced differential expression of proteins that mediate in the early stages of EndMT. A proteomic profile of endothelial cells leading to differentiation into a mesenchymal phenotype showed that some of the 17 overexpressed proteins, such as palladin, torsin A, nuleoporin1 and POTE I, could be considered essential in EndMT. In addition, the Snail and GSK- β signaling pathways were shown to be involved in the upregulation of palladin in TGF-β -induced EndMT. Our results identified palladin as a novel marker in EndMT.

Funding Sources

This project has received funding from the Polish-Norwegian Research Program (MOMENTO Pol-Nor/209521/5/2013).

Competing Interests

The authors declare that they have no competing interests.

Acknowledgement

This work is dedicated to Prof. Czeslaw Cierniewski (1946–2013).

Citation: Stasiak M, Gawryś K, Popielarski M, Bednarek R, Studzian M, et al. (2017) Differential Quantitative Proteomics of Human Microvascular Endothelial Cells 1 by iTRAQ Reveals Palladin to be a New Biomarker During TGF-β1 Induced Endothelial Mesenchymal Transition. J Proteomics Bioinform 10: 236-245. doi: 10.4172/jpb.1000447

References

1. Mendoza FA, Artlett CM, Sandorfi N, Latinis K, Piera-Velazquez S, et al. (2006) Description of 12 cases of nephrogenic fibrosing dermopathy and review of the literature. Semin Arthritis Rheum 35: 238-249.
2. Noble PW (2006) Idiopathic pulmonary fibrosis: natural history and prognosis. Clin Chest Med 27: S11–S16.
3. Bataller R, Brenner DA (2005) Liver fibrosis. J Clin Invest 115: 209-218.
4. Schnaper HW, Kopp JB (2003) Renal fibrosis. Front Biosci 8: e68-86.
5. Rosenbloom J, Castro SV, Jimenez SA (2010) Narrative review: fibrotic diseases: cellular and molecular mechanisms and novel therapies. Ann Intern Med 152: 159-166.
6. Wei J, Bhattacharyya S, Tourtellotte WG, Varga J (2011) Fibrosis in systemic sclerosis: emerging concepts and implications for targeted therapy. Autoimmun Rev 10: 267-275.
7. Wynn TA (2008) Cellular and molecular mechanisms of fibrosis. J Pathol 214: 199-210.
8. Zeisberg EM, Potenta S, Xie L, Zeisberg M, Kalluri R (2007) Discovery of endothelial to mesenchymal transition as a source for carcinoma-associated fibroblasts. Cancer Res 67: 10123-10128.
9. Zeisberg EM, Tarnavski O, Zeisberg M, Dorfman AL, McMullen JR, et al. (2007) Endothelial-to-mesenchymal transition contributes to cardiac fibrosis. Nat Med 13: 952-961.
10. Kalluri R, Zeisberg M (2006) Fibroblasts in cancer. Nat Rev Cancer 6: 392-401.
11. Zeisberg EM, Potenta SE, Sugimoto H, Zeisberg M, Kalluri R (2008) Fibroblasts in kidney fibrosis emerge via endothelial-to-mesenchymal transition. J Am Soc Nephrol 19: 2282-2287.
12. Kokudo T, Suzuki Y, Yoshimatsu Y, Yamazaki T, Watabe T, et al. (2008) Snail is required for TGFβ-induced endothelial mesenchymal transition of embryonic stem cell derived endothelial cells. J Cell Sci 121: 3317-3324.
13. Piera-Velazquez S, Li Z, Jimenez SA (2011) Role of endothelial-mesenchymal transition (EndoMT) in the pathogenesis of fibrotic disorders. Am J Pathol 179: 1074-1080.
14. Bakun M, Niemczyk M, Domanski D, Jazwiec R, Perzanowska A, et al. (2012) Urine proteome of autosomal dominant polycystic kidney disease patients. Clin Proteomics 9:13.
15. Malinowska A, Kistowski M, Bakun M, Rubel T, Tkaczyk M, et al. (2012) Diffprot - software for non-parametric statistical analysis of differential proteomics data. J Proteomics 75: 4062-4073.
16. Li Z, Wermuth PJ, Benn BS, Lisanti MP, Jimenez SA (2013) Caveolin-1 deficiency induces spontaneous endothelial-to-mesenchymal transition in murine pulmonary endothelial cells in vitro. Am J Pathol 182: 325-331.
17. Kitao A, Sato Y, Sawada-Kitamura S, Harada K, Sasaki M, et al. (2009) Endothelial to mesenchymal transition via transforming growth factor-beta1/Smad activation is associated with portal venous stenosis in idiopathic portal hypertension. Am J Pathol 175: 616-626.
18. D-Angelo MA, Hetzer MW (2008) Structure, dynamics and function of nuclear pore complexes. Trends Cell Biol 18: 456-466.
19. Alber F, Dokudovskaya S, Veenhoff LM, Zhang W, Kipper J, et al. (2007) Determining the architectures of macromolecular assemblies. Nature 450: 683-694.
20. Alber F, Dokudovskaya S, Veenhoff LM, Zhang W, Kipper J, et al. (2007) The molecular architecture of the nuclear pore complex. Nature 450: 695-701.
21. Schwartz TU (2005) Modularity within the architecture of the nuclear pore complex. Curr Opin Struct Biol 15: 221-226.
22. Terry LJ, Shows EB, Wente SR (2007) Crossing the nuclear envelope: hierarchical regulation of nucleocytoplasmic transport. Science 318: 1412-1416.
23. Chen X, Xu L (2010) Specific nucleoporin requirement for Smad nuclear translocation. Mol Cell Biol 30: 4022-4034.
24. Bera TK, Saint Fleur A, Lee Y, Kydd A, Hahn Y, et al. (2006) POTE paralogs are induced and differentially expressed in many cancers. Cancer Res 66: 52-56.
25. Wang Q, Li X, Ren S, Cheng N, Zhao M, et al. (2015) Serum levels of the cancer-testis antigen POTEE and its clinical significance in non-small-cell lung cancer. PLoS One 10: e0122792.
26. Redfield SM, Mao J, Zhu H, He Z, Zhang X, et al. (2013) The C-terminal common to group 3 POTES (CtG3P): a newly discovered nucleolar marker associated with malignant progression and metastasis. Am J Cancer Res 3: 278-289.
27. Bera TK, Huynh N, Maeda H, Sathyanarayana BK, Lee B, et al. (2004) Five POTE paralogs and their splice variants are expressed in human prostate and encode proteins of different lengths. Gene 337: 45-53.
28. Nery FC, Armata IA, Farley JE, Cho JA, Yaqub U, et al. (2011) TorsinA participates in endoplasmic reticulum-associated degradation. Nat Commun 2: 393.
29. Nery FC, Zeng J, Niland BP, Hewett J, Farley J, et al. (2008) TorsinA binds the KASH domain of nesprins and participates in linkage between nuclear envelope and cytoskeleton. J Cell Sci 121: 3476-3486.
30. Boukhelifa M, Moza M, Johansson T, Rachlin A, Parast M, et al. (2006) The proline-rich protein palladin is a binding partner for profilin. FEBS J 273: 26-33.
31. Boukhelifa M, Parast MM, Bear JE, Gertler FB, Otey CA (2004) Palladin is a novel binding partner for Ena/VASP family members. Cell Motil Cytoskeleton 58: 17-29.
32. Mykkanen OM, Gronholm M, Ronty M, Lalowski M, Salmikangas P, et al. (2001) Characterization of human palladin, a microfilament-associated protein. Mol Biol Cell 12: 3060-3073.
33. Rachlin AS, Otey CA (2006) Identification of palladin isoforms and characterization of an isoform-specific interaction between Lasp-1 and palladin. J Cell Sci 119: 995-1004.
34. Goicoechea S, Arneman D, Disanza A, Garcia-Mata R, Scita G, et al. (2006) Palladin binds to Eps8 and enhances the formation of dorsal ruffles and podosomes in vascular smooth muscle cells. J Cell Sci 119: 3316–3324.
35. Ronty M, Taivainen A, Moza M, Kruh GD, Ehler E, et al. (2005) Involvement of palladin and alpha-actinin in targeting of the Abl/Arg kinase adaptor ArgBP2 to the actin cytoskeleton. Exp Cell Res 310: 88-98.
36. Ronty M, Taivainen A, Moza M, Otey CA, Carpen O (2004) Molecular analysis of the interaction between palladin and alpha-actinin. FEBS Lett 566: 30-34.
37. Maeda M, Asano E, Ito D, Ito S, Hasegawa Y, et al. (2009) Characterization of interaction between CLP36 and palladin. FEBS J 276: 2775-2785.
38. Parast MM, Otey CA (2000) Characterization of palladin, a novel protein localized to stress fibers and cell adhesions. J Cell Biol 150: 643-656.
39. Ronty MJ, Leivonen SK, Hinz B, Rachlin A, Otey CA, et al. (2006) Isoform-specific regulation of the actin-organizing protein palladin during TGF-beta1-induced myofibroblast differentiation. J Invest Dermatol 126: 2387-2396.
40. Pogue-Geile KL, Chen R, Bronner MP, Crnogorac-Jurcevic T, Moyes KW, et al. (2006) Palladin mutation causes familial pancreatic cancer and suggests a new cancer mechanism. PLoS Med 3: e516.
41. Goicoechea SM, Bednarski B, Stack C, Cowan DW, Volmar K, et al. (2010) Isoform-specific upregulation of palladin in human and murine pancreas tumors. PLoS One 5: e10347.
42. Goicoechea SM, García-Mata R, Staub J, Valdivia A, Sharek L, et al. (2014) Palladin promotes invasion of pancreatic cancer cells by enhancing invadopodia formation in cancer-associated fibroblasts. Oncogene 33: 1265-1273.
43. Morishige N, Murata S, Nakamura Y, Azumi H, Shin-Gyou-Uchi R, et al. (2016) Coordinated regulation of palladin and α–smooth muscle actin by transforming growth factor–β in human corneal fibroblasts. Invest Ophthalmol Vis Sci 57: 3360-3368.
44. Teresa A, Brentnall TA, Lai LA, Coleman J, Bronner MP, et al. (2012) Arousal of cancer-associated stroma: overexpression of palladin activates fibroblasts to promote tumor invasion. PLoS One 7: e30219.

Citation: Stasiak M, Gawryś K, Popielarski M, Bednarek R, Studzian M, et al. (2017) Differential Quantitative Proteomics of Human *Microvascul*ar Endothelial Cells 1 by iTRAQ Reveals Palladin to be a New Biomarker During TGF-β1 Induced Endothelial Mesenchymal Transition. J Proteomics Bioinform 10: 236-245. doi: 10.4172/jpb.1000447